ELSEVIER

International Journal of Mass Spectrometry 223–224 (2003) 237–251

International Journal of Mass Spectrometry

www.elsevier.com/locate/ijms

Experimental evaluation of the recombination rate of cations formed from fluoranthene

C. Rebrion-Rowe*, J.L. Le Garrec, M. Hassouna, D. Travers, B.R. Rowe

Université de Rennes, Physique des Atomes, Lasers, Molécules et Surfaces (P.A.L.M.S.), U.M.R. 6627 du C.N.R.S., 35042 Rennes Cedex, France

Received 4 January 2002; accepted 11 April 2002

Abstract

The recombination of electrons with polycyclic ions produced via ion–molecule reactions between N^+ and $N_2{}^+$ precursor ions and fluoranthene ($C_{16}H_{10}$) has been studied at 300 K using a flowing afterglow Langmuir probe-mass spectrometer (FALP-MS) apparatus. The primary ions produced from these ion–molecule reactions consisted of pure hydrocarbon cations, and nitrogen-bearing compounds. These primary ions reacted further with fluoranthene to give adduct ions. As pyrene, which was present as an impurity in fluoranthene, attaches electrons, and for other reasons that are discussed in the paper, we have modeled the chemistry in our flow, in order to determine the recombination rates of the primary and the secondary ions with electrons. The fitted value for our primary ions is $(2.5 \pm 1.5) \times 10^{-6}\,cm^3\,s^{-1}$ and the recombination rate for the secondary ions is close to the physical limit. (Int J Mass Spectrom 223–224 (2003) 237–251)

Keywords: Recombination; Fluoranthene; Ions

1. Introduction

Polycyclic aromatic hydrocarbons (PAHs) are among the most ubiquitous organic compounds in the universe. They are found in terrestrial environments, such as sediments [1], in air as carcinogenic pollutants [2] due to anthropic emissions from for example, diesel exhaust [3] as well as in extraterrestrial media, such as meteorites [4] and interstellar space [5] where PAH cations might be good candidates as the carriers of the diffuse interstellar bands [6].

The chemistry responsible for the formation or the destruction of PAHs in the gas phase is not well understood. A lot of chemical networks have been built up to explain soot formation in flames or in the pyrolysis of hydrocarbons, that involve neutral PAHs and their cations (see for example [7–10]). These models remain to be confirmed by experimental measurements and to our knowledge, the actual mechanisms for PAH formation, in interstellar space and in flames, are still unknown.

Nevertheless, the presence of PAHs on earth is a matter of fact, and if there is no definitive proof that PAHs are present in the interstellar medium, there is some experimental evidence for large aromatic molecules in space [11–13]. Typical CC and CH stretching and bending modes of PAHs match strong bands that are observed between 3 and 25 μm in the

* Corresponding author. E-mail: christiane.rebrion@univ.rennes.fr

1387-3806/02/$ – see front matter
PII S1387-3806(02)00794-7

infrared emission spectra of many interstellar objects [14–16]. According to the intensities of these spectral features, which are relatively invariant with respect to specific PAH species, but are sensitive to their ionisation state, PAHs should occur predominantly in their cationic form [17,18]. In particular, a feature at 16.4 μm can be attributed to a molecule belonging to the low-mass end of the interstellar PAH distribution [16]. This is possibly fluoranthene [15], the molecule of interest in this paper. This transition could, however, be due to silicon nanoparticles [19] or silicates [20].

The experimental study of isolated PAH cations is a challenge. Recent advances have been made in spectroscopy as visible [21–23] and infrared spectra [24] of PAH cations having up to 16 carbon atoms have been recorded. No definitive identification of interstellar PAHs has, however, occurred, possibly because the studied species are too small to survive photodissociation in the interstellar medium [25,26]. Another reason could be that these small PAH cations react rapidly with species that are abundant in the interstellar medium. Ion–molecule reactions involving PAH cations and the atoms N, O and with the very abundant H atom, have for example shown that association channels can be prominent [27]. Electrons are also supposed to be abundant, and could efficiently destroy PAH cations by electron–ion recombination. We report here results on the recombination of cations formed from fluoranthene.

2. Experimental

2.1. Description of the apparatus

The technique is an extension of a classic flowing afterglow Langmuir probe (FALP) technique that includes a moveable mass spectrometer (MS), which is used to identify the ions and to measure their relative densities as a function of distance along the flow. The apparatus has been described extensively elsewhere [28] and only the details specific to the study of the cations formed from fluoranthene will be given in this paper.

In the apparatus (Fig. 1), an afterglow is formed in a helium buffer gas which is introduced at a flow rate of 21.7 sl min^{-1}. This afterglow contains neutral ground state and metastable excited state helium atoms He^M ($2\ ^3S$), He^+, and He_2^+ ions. The measurements reported here were performed at a helium density of about 10^{16} cm^{-3}. Under these conditions, the hydrodynamic measuring time was 1 ms with a flow velocity $v = 1.13 \times 10^4$ cm s^{-1} and the initial electron density was varied from 8×10^8 to 8×10^9 cm^{-3}. N_2 was chosen as precursor gas to form the ions to be studied, as reactions of N_2^+ and N^+ with smaller aromatic hydrocarbons like naphthalene [29] are mainly pure charge transfer and do not exhibit insertion of the nitrogen atom into the hydrocarbon molecule. It was expected that this should also

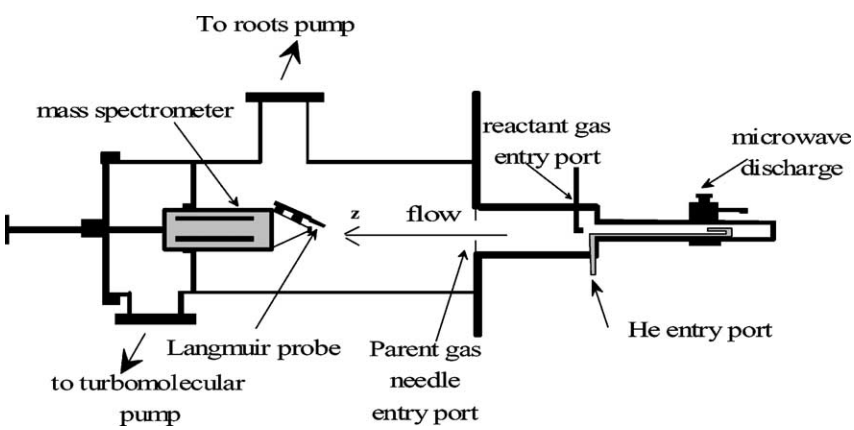

Fig. 1. The FALP-MS apparatus.

be the case for larger PAHs. N_2 was introduced at a second entry port at about 0.1 sl min^{-1}, downstream of the microwave cavity. It reacts by ion–molecule reactions with He^+ and $He_2{}^+$ [30]:

$$He^+ + N_2 \rightarrow He + N_2{}^+ \ (44\%)$$
$$\rightarrow He + N^+ + N \ (56\%),$$
$$k_1 = 1.5 \times 10^{-9}\ cm^3\ s^{-1}$$

$$He_2{}^+ + N_2 \rightarrow 2He + N_2{}^+,$$
$$k_2 = 1.3 \times 10^{-9}\ cm^3\ s^{-1}$$

and the metastable helium atoms He^M ($2\ ^3S$) are destroyed by Penning ionisation [31]:

$$He^M + N_2 \rightarrow N_2{}^+ + e + He,$$
$$k_3 = 8 \times 10^{-11}\ cm^3\ s^{-1}$$

so as to produce a plasma dominated by $N^+/N_2{}^+$. $N_2{}^+$ is at least partially removed by dissociative recombination ($\alpha = 2.6 \times 10^{-7}\ cm^3\ s^{-1}$ [32]).

The parent vapour of the ion to be studied was introduced through the needle entry port, located further downstream. At this point, the mass spectrometer confirmed that the plasma contained no He^+ or $He_2{}^+$, and consisted a mixture of N^+ and $N_2{}^+$, the ratio $N_2{}^+/N^+$ depending upon the initial electron density. This point is usually taken as the arbitrary origin z_0 for our chemical reactions.

2.2. The injection of fluoranthene

Fluoranthene ($C_{16}H_{10}$) was provided by Sigma–Aldrich at 98% purity, and was used without further purification. (The major impurity is pyrene, a structural isomer of fluoranthene (Fig. 2).)

At room temperature, $C_{16}H_{10}$ is a white solid. It melts at about 383 K (110 °C), a temperature at which its vapour pressure is only a few millitorr (mTorr). It was vaporised upstream of the needle injector in an oven, whose temperature was maintained constant, at 140 °C. At this temperature, the vapour pressure is less than 1 Torr. The values of vapour pressure given here are only orders of magnitude, and are deduced from an extrapolation of data available for temperatures greater than 400 K [33]. The vapours were flushed into the needles by a helium flow, which could be adjusted, as could the total pressure in the oven.

The fluoranthene flow rate q_{fluo} is linked to the total (measured) pressure P_{oven} in the oven, the fluoranthene vapour pressure P_{fluo} at the temperature of the oven and to the helium flow rate through the oven q_{He} by:

$$q_{fluo} = q_{He} \frac{P_{fluo}}{P_{oven} - P_{fluo}} \quad (1)$$

As the total pressure in the oven was at least 350 Torr, and the vapour pressure of fluoranthene less than 1 Torr, this expression can be simplified and

$$q_{fluo} \cong q_{He} \frac{P_{fluo}}{P_{oven}} \quad (2)$$

The helium flow rate through the oven was regulated by Tylan flowmeters. All the gas lines between the oven and the needles were heated, the upstream parts being cooler than the downstream ones, and the needles themselves were heated ohmically.

2.3. Protection of the measurement tools

Once injected, a non-negligible part of the fluoranthene is not ionised and stays in its neutral form, and as the experiment chamber is at room temperature,

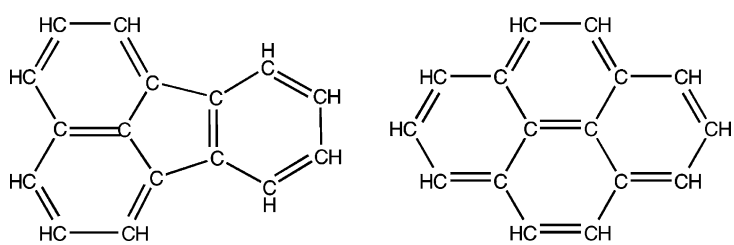

Fig. 2. Semi-developed formulas of fluoranthene (left) and pyrene (right).

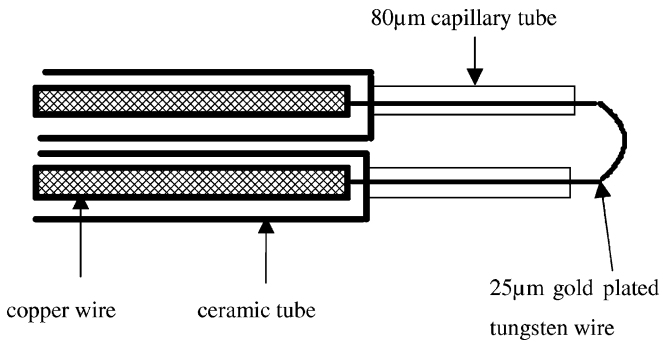

Fig. 3. The modified Langmuir probe. The capillary tubes had to be removed.

re-deposits on all surfaces. In order to keep our Langmuir probe and the sampling orifice of the mass spectrometer operational, we cleaned them by heating.

Our modified Langmuir probe (Fig. 3) has been described in detail elsewhere [34]. Basically it consists of a loop of a very thin, gold plated tungsten wire which collects electrons from the plasma, provided a suitable bias voltage is applied. A continuous current of 100–150 mA heats the wire, and is superimposed upon the current due to electron collection. This current cleaned the probe when fluoranthene is re-deposited, but also heated the capillary tubes. These capillary Pyrex tubes were used to have a well-defined probe length, as only the surface of the gold wire outside the capillary collects electrons. The hydrocarbon, however, which was deposited on the capillary underwent a kind of polymerisation and/or pyrolysis process, forming a black current conducting surface, which happened to be in contact with the probe, thus increasing the collecting surface. This probe shift was noticeable when measuring the dissociative recombination rate of O_2^+ before and after using PAH cations. At the end of the experiment, it was as much as three times lower than the accepted value of $1.8 \times 10^{-7}\,cm^3\,s^{-1}$ [35] which was measured when the probe was new. To avoid this shift, the capillary tubes were eliminated, and the wire exited directly from a small ceramic tube (about 500 μm in internal diameter).

The other surface that had to be protected was the sampling orifice of the mass spectrometer, which is a fraction of a millimetre in diameter. In order to avoid deposition of solid material, an electrical wire was wrapped around the entrance cone of the mass spectrometer and a temperature probe was used to pilot the heating for setting the cone temperature at 150 °C. A circulating water jacket protected the remainder of the mass spectrometer from heating.

2.4. Measurement of the rate coefficient

The FALP-MS method usually allows the measurement of the recombination rate of an individual ion, even if other ions are present in the flow which undergo recombination also, and even if the ion of interest reacts via ion–molecule reactions. This method has been used in our former studies of the dissociative recombination of saturated and unsaturated hydrocarbons [36–38] and the interested reader will find the details in the cited articles. To understand why this method could not be used here, its basis must be recalled.

Let M_i^+ be the ion whose recombination is studied. The ion–molecule reaction of the precursor ions (P^+) with the neutral parent of the ion under study gives what we call the primary ions. M_i^+ is usually among these primary ions:

$$P_i^+ + C_{16}H_{10} \xrightarrow{k_i} M_i^+ + \text{fragments}$$

Further reactions of M_i^+ with other neutrals (N_j) present in the flow, mainly the neutral parent itself and impurities if any, give secondary ions (sec^+):

$$M_i^+ + N_j\,(+B) \xrightarrow{k_j} sec^+ + \text{fragments}\,(+B)$$

where k_j is an effective bimolecular rate constant and B the buffer gas.

M_i^+ decays also by reaction with electrons (recombination rate α_i):

$$M_i^+ + e \xrightarrow{\alpha_i} \text{products}$$

Taking ambipolar diffusion into account, the equation governing the evolution of $[M_i^+]$ vs. time is:

$$\frac{d[M_i^+]}{dt} = v\frac{d[M_i^+]}{dz} = \underbrace{\sum_i k_i[P_i^+][C_{16}H_{10}]}_{\text{production}} - \underbrace{\sum_j k_j[M_i^+][N_j]}_{\text{ion–molecule reactions}} - \underbrace{\alpha_i[M_i^+][e]}_{\text{DR}} - \underbrace{\frac{D_A}{\Lambda^2}[M_i^+]}_{\text{diffusion}} \quad (3)$$

Provided that M_i^+ is not produced in the recombination zone (i.e., the precursor ions are completely destroyed), Eq. (3) can be integrated:

$$\ln\frac{[M_i^+]_z}{[M_i^+]_{z_0}} = -\frac{\alpha_i}{v}\int_{z_0}^{z}[e]dz - \frac{1}{v}\left(k_j[N_j] + \frac{D_A}{\Lambda^2}\right)(z - z_0) \quad (4)$$

where z_0 is the initial position of the mass spectrometer and the Langmuir probe, and z any position downstream. The DR rate can be obtained by plotting $\ln([M_i^+]_{z_1}/[M_i^+]_{z_0})$ vs. $(1/v)\int_{z_0}^{z_1}[e]\,dz$ at a fixed position, z_1 for different initial electron densities. One obtains a straight line, its slope gives the recombination rate, and the term representing other losses than recombination is a constant.

This plot, however, requires that $[M_i^+]_{z_1}/[M_i^+]_{z_0}$ is measured. This is usually achieved by measuring the molar fraction $x_i = [M_i^+]/\sum_i[M_i^+]$ from the mass spectrum, and $[M_i^+]$ is then calculated from the equality:

$$\sum_i [M_i^+]_z = [e]_z \quad (5)$$

This is true if no electron attachment occurs.

To summarise, to be valid, the mathematical equations that lead to the recombination rate require firstly,

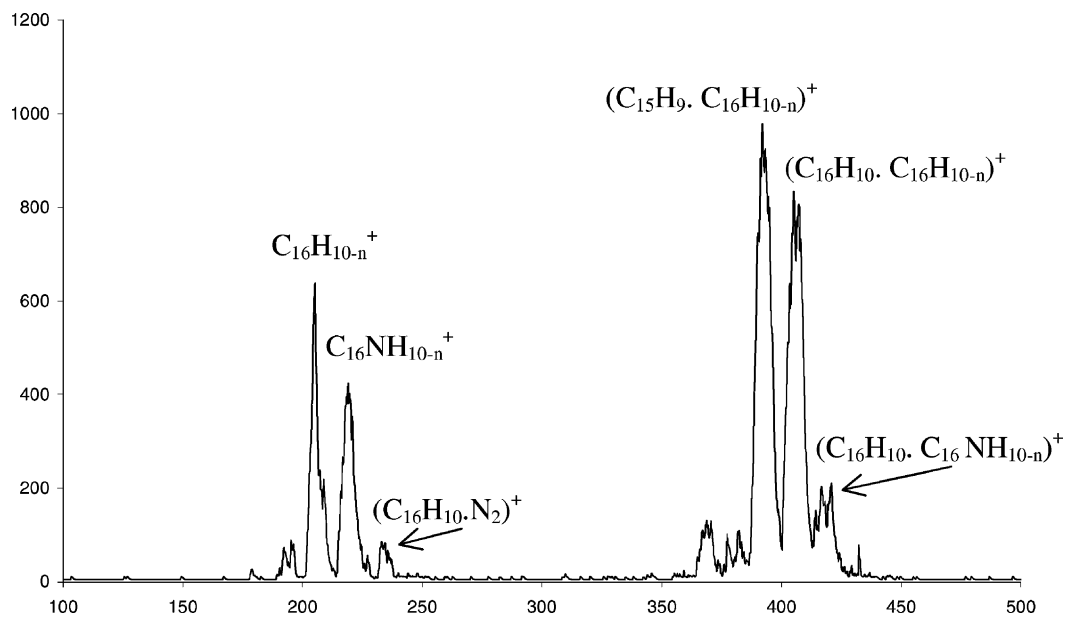

Fig. 4. Typical mass spectrum (positive ions) in the 100–500 mass range, recorded at high resolution with the maximum fluoranthene flow rate.

the precursor ions must be destroyed, secondly, no electron attachment must occur, and finally, one must be able to deduce the relative ion densities from mass spectrum.

Unfortunately, all three conditions were violated here. If conditions were such that all the precursor ions were destroyed by ion–molecule reactions, $C_{16}H_{10}^{+}$ was also almost totally converted into the adduct ($C_{16}H_{10}^{+}\cdot C_{16}H_{10}$), whose production is enhanced when the amount of $C_{16}H_{10}$ is increased. Conversely, when the fluoranthene flow rate was kept low so that only $C_{16}H_{10}^{+}$ were found in the flow, the precursor ions were also present. The second problem is that the ions present in the flow ranged from mass 14 to 450 (Fig. 4). With such mass ranges, mass discrimination makes it impossible to determine the relative densities of numerous individual ions. This phenomenon is well known from mass spectrometer users, and consists in a distorted representation of the peak heights in the mass spectrum, according to the mass of the ions. Depending upon the power supply (Balzers or Extranuclear) used for the mass spectrometer, we observe different mass discrimination behaviours. The Balzers power supply works for masses between 0 and 300 and enhances the low masses, and the Extranuclear power supply (high-Q head model 15) is used for masses ranging from 0 to 1000 and favours the high masses (in fact, masses lower than 50 are hardly seen).

Last but not least, negative $C_{16}H_{10}^{-}$ was present in the flow, which is the product of the non-dissociative electron attachment to pyrene [39], the impurity present in fluoranthene. For these reasons, a model of the chemistry has been made, which is based on the measurement of the electron density. This parameter was chosen because it was measured in the most reliable way.

3. Modelling

3.1. Reaction network

According to the works of Ling and Lifshitz [40] and Jochims et al. [41], the charge transfer reactions (6) and (7) are exothermic enough to induce H or H_2 loss, leading to $C_{16}H_{10-n}^{+}$ with $n = 0$, 1 or 2. Obviously some $C_{16}H_{10-n}N^{+}$ is formed (Fig. 4), proving that a nitrogen atom can be added to a hydrocarbon skeleton. The mass spectrum shows that cations containing less than 16 carbon atoms are also present (Fig. 5). In our modelling, we have separated the cations into two groups: the primary one ($prim^{+}$) and formed from the precursor ions, and the secondary one (sec^{+}), resulting from ion–molecule reactions of the primary cations with neutral fluoranthene.

In the frame of these drastic simplifications, we have modelled the chemistry with the following chemical network:

$$N^{+} + C_{16}H_{10} \xrightarrow{k_1} prim^{+} + \text{fragments} \quad (6)$$

$$N_2{}^{+} + C_{16}H_{10} \xrightarrow{k_2} prim^{+} + \text{fragments} \quad (7)$$

$$prim^{+} + C_{16}H_{10}(+M) \xrightarrow{k_3} sec^{+}(+M) \quad (8)$$

$$prim^{+} + e \xrightarrow{\alpha_1} \text{products} \quad (9)$$

$$sec^{+} + e \xrightarrow{\alpha_2} \text{products} \quad (10)$$

$$N_2{}^{+} + e \xrightarrow{\alpha_3} N + N \quad (11)$$

$$C_{16}H_{10}\ (\text{pyrene}) + e \xrightarrow{\beta} C_{16}H_{10} \quad (12)$$

Ion–ion recombination was neglected because the negative ions were produced in small amounts, and because ion–ion recombination reactions are usually slower (less than $10^{-7}\,cm^3\,s^{-1}$ [42]) than electron–ion recombination reactions.

Rate constants k_1, k_2, and k_3 (effective binary rate constant) are deduced from the experiments, α_3 is well known and α_1, α_2, and β will be the adjustable parameters of the model.

3.2. Preliminary experiments

3.2.1. The ion–molecule reactions

Fluoranthene has a small dipole moment (0.35 D) and its polarisability is $\alpha = 29.3 \times 10^{-24}\,cm^3$ (A. Boucekkine, personal communication). It is, therefore, expected to react at 300 K with N^{+} and $N_2{}^{+}$ at the

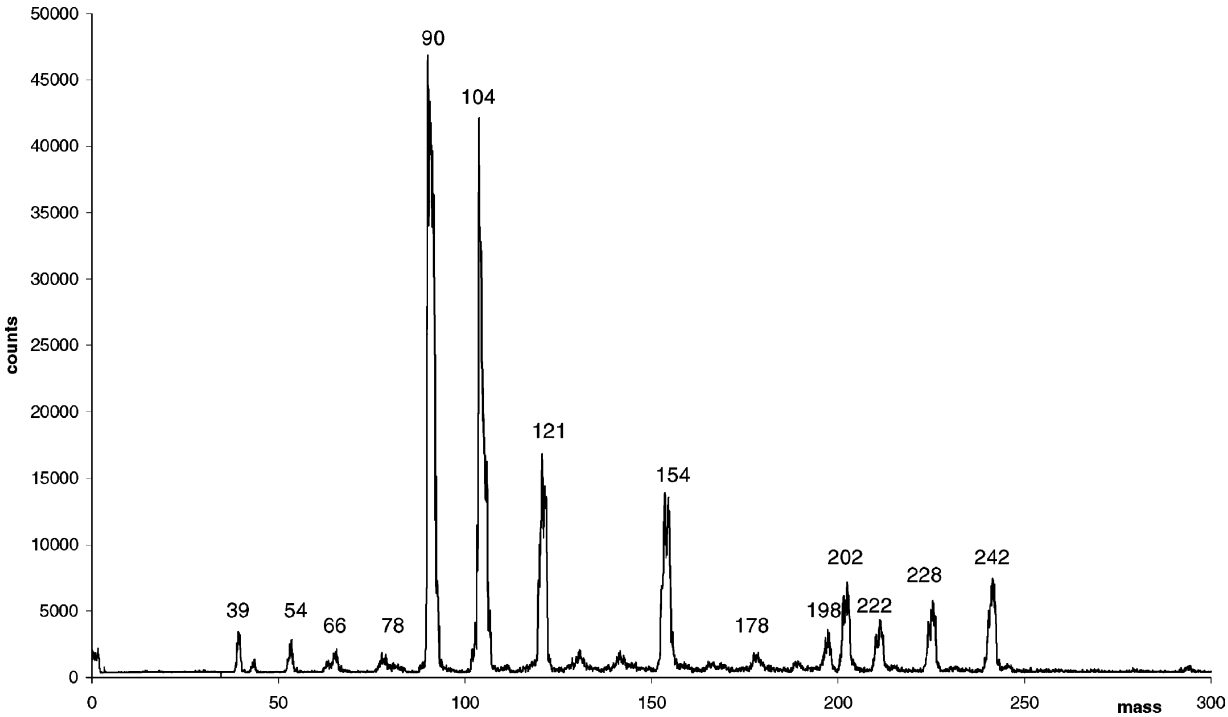

Fig. 5. Detail of the low mass part of the spectrum (positive ions). Because of mass discrimination, the peaks at higher masses appear smaller than they actually are. Labels are assigned to the tip of the peaks.

Langevin rates which are: $k_{L1} = 3.5 \times 10^{-9}$ and $k_{L2} = 2.5 \times 10^{-9}$ cm^3 s^{-1} and the second-order rate constant corresponding to the association reaction (8) is $k_3 = 1.3 \times 10^{-9}$ cm^3 s^{-1}.

Let us consider the reaction $P^+ + C_{16}H_{10} \xrightarrow{k}$ products, P^+ represent N^+ or $N_2{}^+$. At low electron density, the dissociative recombination of $N_2{}^+$ can be neglected as a loss channel for $N_2{}^+$, and the decay of $[P^+]$ vs. distance is due to ion–molecule reactions and diffusion loss:

$$\frac{d[P^+]}{dt} = v\frac{d[P^+]}{dz} = -k[P^+][C_{16}H_{10}] - \frac{[P^+]}{\tau_{diff}}$$

where τ_{diff} is the diffusion time.

We have measured the decay of $[P^+]$ vs. the distance along the axis of the flow, z (Fig. 7). As the velocity of the flow, v, is constant,

$$\ln[P^+] = \left(-k[C_{16}H_{10}] - \frac{1}{\tau_{diff}}\right)\frac{z - z_0}{v} + \ln[P^+]_0$$

and $\ln[P^+]$ as a function of z is a straight line whose slope is $-(1/v)\{k[C_{16}H_{10}] + (1/\tau_{diff})\}$.

If one knew exactly the fluoranthene density in the flow, which is in fact the total density injected through the needles, one could plot this slope vs. $[C_{16}H_{10}]$ and deduce k, as is usually done. The problem here is that no reliable data on the vapour pressure of fluoranthene are available at the temperatures at which the oven was heated.

To overcome this difficulty, we have worked with the temperature of the oven fixed at 140 °C, therefore, fixing the fluoranthene vapour pressure P_{fluo}. According to Eq. (2), the fluoranthene flow rate, and consequently its density, is directly proportional to the ratio (q_{He}/P_{tot}), which is well defined. We have made three measurements of the decay of $\ln[P^+]$ vs. z, the fluoranthene density being varied by varying the total pressure, and one measurement without fluoranthene. The slope of these decays as a function of q_{He}/P_{tot}

give $k_1 P_{\text{fluo}} = 1.53 \times 10^{-9}\,\text{cm}^3\,\text{s}^{-1}$ Torr for N^+ and $k_2 P_{\text{fluo}} = 1.03 \times 10^{-9}\,\text{cm}^3\,\text{s}^{-1}$ Torr for $N_2{}^+$, the value of τ_{diff} being 1.36 ± 0.7 ms. It has to be noted that

$$\frac{k_1 P_{\text{fluo}}}{k_2 P_{\text{fluo}}} \cong \sqrt{\frac{\mu_2}{\mu_1}}$$

where μ is the reduced mass of the ion–molecule system, as is expected for a reaction that occurs at the collisional rate.

If one agrees that these reactions occur at the Langevin rate, the vapour pressure of fluoranthene can be estimated to be 0.425 ± 0.025 Torr, a value which is consistent with the extrapolated values from higher temperatures.

Provided that all experiments are done with the temperature of the oven set at 140 °C, these data can be used for modelling.

3.2.2. Diffusion time

In our determination of the ion–molecule reactions rates, we have determined the diffusion time for N^+ which is $\tau_{\text{diff}} = 1.36$ ms. In our flow, the diffusion is ambipolar, and the diffusion time varies roughly as the reduced mass of the ion and the buffer gas which is helium. In our experiment, the reduced mass varies from 3.1 amu (N^+) to 3.9 amu ($(C_{16}H_{10})_2{}^+$) so that if one considers that the diffusion time is the same for all ions, the error in this term is less than 30%. In our model, we have given the same value to all diffusion times, which is the value determined for N^+. The only case, however, for which the diffusion term is not small compared to the other losses and necessary to reproduce the experimental results, is the decay of N^+ when the fluoranthene flow rate is very small.

3.2.3. Electron attachment to pyrene

Fluoranthene and pyrene both have positive-electron affinities of $E_{\text{a,fluo}} = 0.63$ eV and $E_{\text{a,pyr}} = 0.591$ eV, respectively [43,44].

Tobita et al. [39] have studied electron attachment on selected PAH molecules, using an energy selected electron beam and detecting the formation of negative-ion resonances as a function of electron energy. They have found that pyrene displays a resonance at zero energy with a small cross-section $\sigma = 1.5 \times 10^{-17}\,\text{cm}^2$. Fluoranthene has a greater attachment cross-section $\sigma = 1.1 \times 10^{-15}\,\text{cm}^2$, but the resonance occurs above zero energy, at 0.25 eV, so we do not expect it to attach electrons at room temperature.

The same situation prevails for the two $C_{14}H_{10}$ isomers, anthracene, and phenantrene, that both have positive-electron affinities and similar cross-sections for attachment, but only anthracene attaches efficiently electrons. The measured value [45] for the electron attachment rate to anthracene at room temperature is $10^{-9}\,\text{cm}^3\,\text{s}^{-1}$.

In our experiment, electron attachment was revealed by the distortion of the positive part of the Langmuir probe *I–V* characteristic, and the negative-ion mass spectrum exhibited two peaks, at masses 202 and 216 (Fig. 6). The first one corresponds to pyrene and its ^{13}C isotope, the second anion is $C_{16}H_{10}N^-$. For the same reasons as above, i.e. the actual pyrene density is unknown, only the pseudo first-order rate β[pyrene] can be determined from our experiments.

3.3. Values of recombination-rate coefficients

The chemical network gave rise to a set of five differential equations representing the time evolution of five chemical species: N^+, $N_2{}^+$, prim^+, sec^+, and e:

$$\frac{\text{d}[N^+]}{\text{d}t} = -k_1[N^+][C_{16}H_{10}] - \frac{[N^+]}{\tau_{\text{diff}}}$$

$$\frac{\text{d}[N_2{}^+]}{\text{d}t} = -k_2[N_2{}^+][C_{16}H_{10}] - \alpha_3[N_2{}^+][\text{e}] - \frac{[N_2{}^+]}{\tau_{\text{diff}}}$$

$$\frac{\text{d}[\text{prim}^+]}{\text{d}t} = (k_1[N^+] + k_2[N_2{}^+] - k_3[\text{prim}^+]) \times [C_{16}H_{10}] - \left(\alpha_1[\text{e}] + \frac{1}{\tau_{\text{diff}}}\right)[\text{prim}^+]$$

$$\frac{\text{d}[\text{sec}^+]}{\text{d}t} = k_3[\text{prim}^+][C_{16}H_{10}] - \left(\alpha_2[\text{e}] + \frac{1}{\tau_{\text{diff}}}\right)[\text{sec}^+]$$

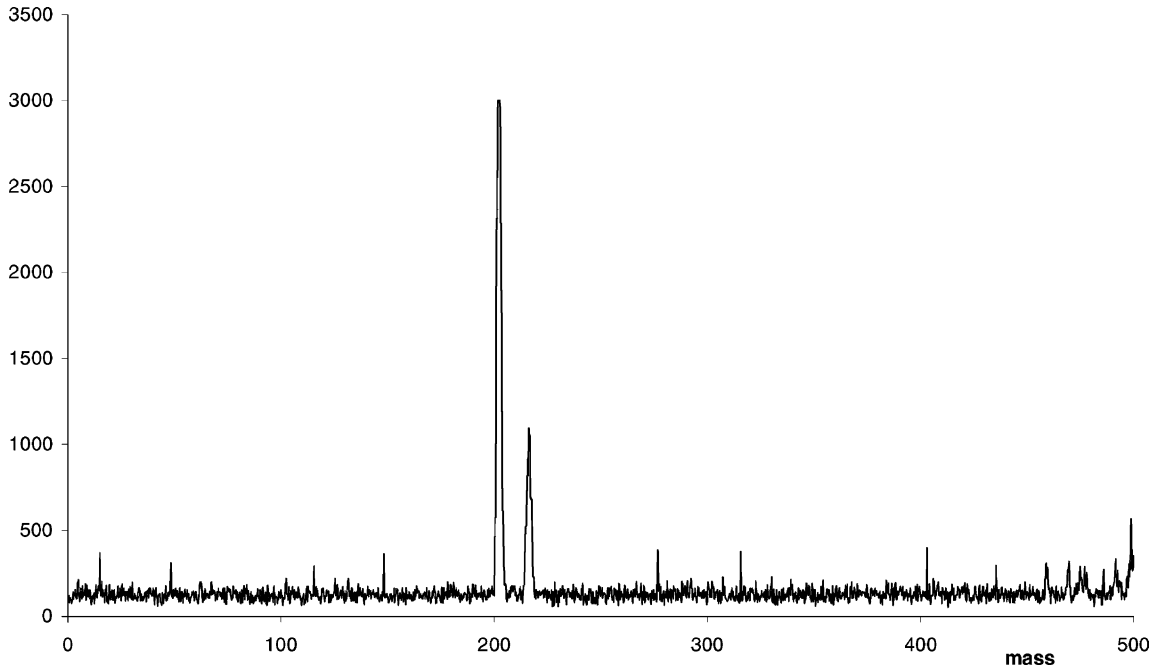

Fig. 6. Mass spectrum of the anions.

$$\frac{\mathrm{d[e]}}{\mathrm{d}t} = -\left(\alpha_1[\mathrm{prim}^+] + \alpha_2[\mathrm{sec}^+] + \alpha_3[{N_2}^+] + \beta[\mathrm{pyrene}] + \frac{1}{\tau_{\mathrm{diff}}}\right)[\mathrm{e}]$$

The pseudo first-order rate coefficient $k_1[C_{16}H_{10}]$ and $k_2[C_{16}H_{10}]$ are measured as well as the diffusion loss time for N^+. The pseudo first-order rate coefficient $k_3[C_{16}H_{10}]$ for the primary ions reacting with fluoranthene, is evaluated from the experimental value for N^+, considering that all ion–molecule reactions occur at the collisional rate. If one considers that the fluoranthene cation is the major primary ion, $k_3 = 0.36k_1$. The rate coefficient for ${N_2}^+$ recombination was taken from the literature values as being equal to $2 \times 10^{-7}\,\mathrm{cm^3\,s^{-1}}$.

The values of the rate coefficients α_1 and α_2 are the unknown coefficients that we want to determine. The electron density was the parameter that was measured in the most reliable way, so we have compared experimental evolutions of electron density with the results of numerical simulation. Four adjustable parameters, α_1, α_2, the pseudo first-order electron attachment rate β[pyrene] and the initial time were used in the numerical simulation.

As the needles are radial to the flow, the fluoranthene vapour is injected perpendicular to the flow axis and induces aerodynamical perturbations. In addition to these perturbations that affect locally the velocity of the flow, the fluoranthene density at the injection port is greater than downstream. Consequently, the precursor ion density decreases much more rapidly during the first centimetre after injection, than it does further downstream when the flow is homogeneous again. This is why the apparent initial reaction time does not correspond to the injection port, located at $z = 0$. The experimental decays of N^+ vs. the distance along the flow-axis z for various fluoranthene flow rates (Fig. 7) allow us to determine an apparent initial position, at which the reactions virtually start. The uncertainty in this position is quite large, and the initial time t_0 was, therefore, kept as an adjustable parameter in the limit of this uncertainty.

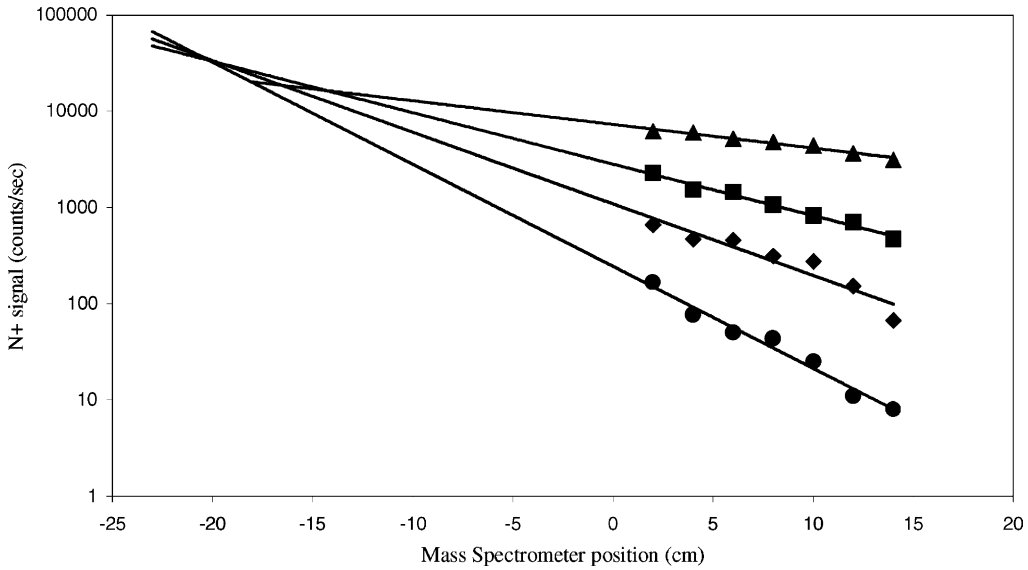

Fig. 7. Decay of the N^+ ions as a function of distance, at different fluoranthene flow rates. (▲): $[C_{16}H_{10}] = 0$; (■): $[C_{16}H_{10}] = 3.41 \times 10^{11} \times P_{fluo}$ (Torr); (◆): $[C_{16}H_{10}] = 5.83 \times 10^{11} \times P_{fluo}$ (Torr); (●): $[C_{16}H_{10}] = 12.5 \times 10^{11} \times P_{fluo}$ (Torr), where P_{fluo} (Torr) is the vapour pressure of fluoranthene at 140 °C, expressed in Torr and $[C_{16}H_{10}]$ is in cm^{-3}.

The set of differential equations was solved for the various initial conditions using a Matlab® routine for stiff equations. The goal was to find the set of adjustable parameters (α_1, α_2, β[pyrene], t_0) that minimised the deviations between the experimental data and numerical results with a mean least-square method. The experimental results consisted of nine decays of the electron density vs. z, with various initial electron densities and fluoranthene flow rates and the experimental conditions are summarised in Table 1. The choice of a larger number of experimental sets, compared to what is mathematically required, increases the constraints on the parameters, which also have to be physically realistic.

In particular, the recombination rates cannot exceed the maximum value α_{max} which can be evaluated [46,47] from the Spitzer formula [48] which gives the recombination cross-section for an ion of radius a (Å):

$$\alpha_{max}\ (cm^3\ s^{-1}) = 1.58 \times 10^{-10} a^2 \sqrt{T} \times \left(1 + \frac{1.665 \times 10^5}{aT}\right)$$

This formula takes into account the planarity of the PAH, which reduces the cross-section by a factor of 0.80 at 300 K. As the C–C distance is ≈1.4 Å, fluoranthene can be included in a circle of radius a = 3.5 Å. This value is close to the radius calculated by Omont for a PAH having N_c carbon atoms, which is

Table 1
Experimental conditions used for the modelling, sorted by increasing initial electron density $[e]_{z_0}$

Initial electron density $[e]_{z_0}$ (cm^{-3})	$\{[N_2^+]/([N_2^+]+[N^+])\}_{z_0}$	$[C_{16}H_{10}]_{z_0}$
8.60×10^8	1	$2.07 \times 10^{11} \times P_{fluo}$
8.60×10^8	1	$2.72 \times 10^{11} \times P_{fluo}$
1.42×10^9	1	$1.15 \times 10^{11} \times P_{fluo}$
1.42×10^9	1	$1.65 \times 10^{11} \times P_{fluo}$
2.30×10^9	0.95	$2.07 \times 10^{11} \times P_{fluo}$
3.50×10^9	0.70	$1.15 \times 10^{11} \times P_{fluo}$
5.77×10^9	0.21	$2.07 \times 10^{11} \times P_{fluo}$
5.77×10^9	0.21	$2.72 \times 10^{11} \times P_{fluo}$
8.50×10^9	0.03	$2.65 \times 10^{11} \times P_{fluo}$

The relative density of the precursor ions $\{[N_2^+]/([N_2^+]+[N^+])\}_{z_0}$ is a function of the electron density, the injected $C_{16}H_{10}$ density is proportional to the fluoranthene vapour pressure at 140 °C expressed in Torr (see text).

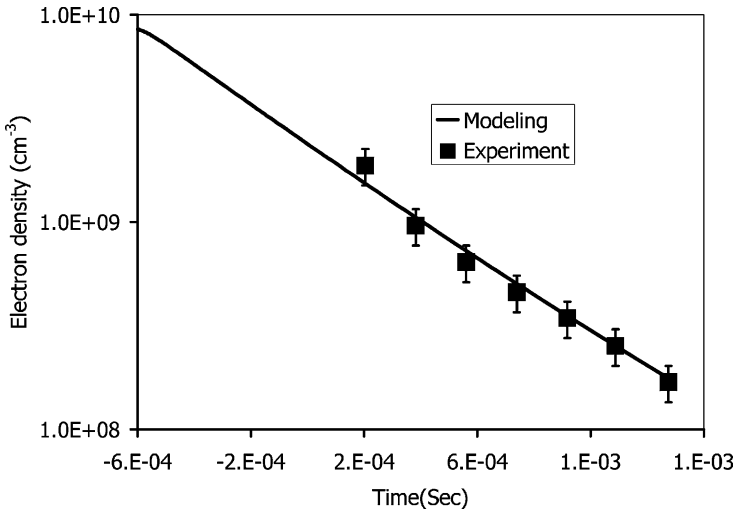

Fig. 8. Comparison of calculated and experimental data for $\alpha_1 = 3 \times 10^{-6}$, $\alpha_2 = 1 \times 10^{-5}$, and $\beta = 1 \times 10^{-9}\,\mathrm{cm^3\,s^{-1}}$. Error bars are 20%.

$a\,(\text{Å}) = 0.9\sqrt{N_c}$. The neutral dimer of fluoranthene can adopt different geometries [49] and its maximum length is ≈13 Å, which can be included in a circle of radius $a = 7$ Å. Assuming that the geometry of the cation is roughly the same as the geometry of the neutral, the recombination rate for the dimer cannot exceed $1.1 \times 10^{-5}\,\mathrm{cm^3\,s^{-1}}$. The same calculation gives $5.3 \times 10^{-6}\,\mathrm{cm^3\,s^{-1}}$ for the monomer.

The search for minimum has been performed by manual iteration, by a "choose and test" procedure and the optimal values were found by successive guesses. Fig. 8 shows a typical fit of one set of experimental data. The optimal value for α_1 was found in the range $(2.5 \pm 1.5) \times 10^{-6}\,\mathrm{cm^3\,s^{-1}}$. We are confident in this result as all searches converged towards the same interval. The uncertainty represents the spread of the numerical results.

At the same time, the rate coefficient for the recombination of the secondary ions was found to vary from $\alpha_2 = 10^{-5}\,\mathrm{cm^3\,s^{-1}}$ to values too large to be acceptable. It is difficult to bracket the value, but as the minimum mathematical value is close to the maximum physical one, one can deduce that the recombination of these ions is fast and close to the physical limit.

4. Discussion

4.1. The primary ions

Fig. 9 shows a mass spectrum recorded close to the injection port, with a small fluoranthene flow rate. The precursor ions N^+ and $N_2{}^+$ are still present, the main product peak is around mass 202 and some fragmentation can be noticed. Our resolution does not allow us to determine if the peak at mass 202 corresponds to a single ion, but energetic considerations can give us some indications.The charge transfer reactions between N^+ and $N_2{}^+$ and neutral fluoranthene are exothermic:

$$N^+ + C_{16}H_{10} \rightarrow C_{16}H_{10}{}^+ + N + 6.63\,\mathrm{eV}$$

$$N_2{}^+ + C_{16}H_{10} \rightarrow C_{16}H_{10}{}^+ + N_2 + 7.68\,\mathrm{eV}$$

In their study of the photodissociation of gas-phase aromatic hydrocarbon cations, Ekern et al. [50] have exposed fluoranthene cations to a xenon-arc lamp emitting photons of energy less than 6.71 eV. In this radiation field, the fluoranthene cation lost up to four hydrogen atoms. As the energy of the photons is very close to the energy released by the ion–molecule reactions, $C_{16}H_{10-n}{}^+$ ions, with n ranging from 0 to 4,

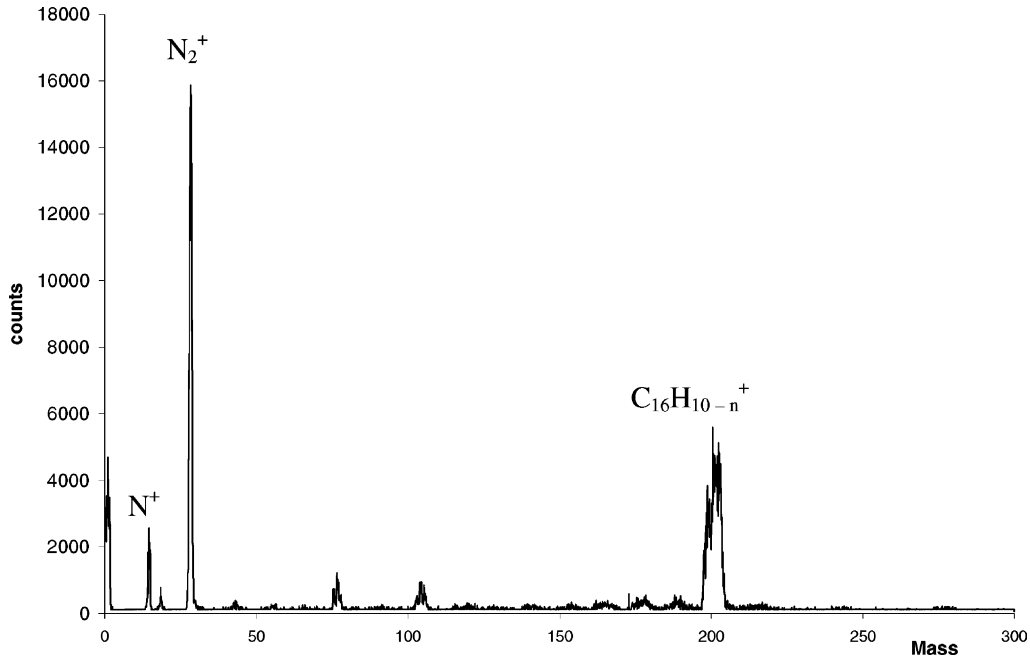

Fig. 9. Mass spectrum of the positive ions recorded close to the needles, with a low fluoranthene flow rate.

can be formed by ion–molecule reaction of neutral fluoranthene with the precursor ions. In our study of the dissociative recombination of cations formed from toluene, we have shown that H atom loss occurs prior to recombination, so that $C_{16}H_{10-n}{}^+$ ions are expected to be primary ions.

C_2H_2 loss is also a fragmentation path for many of PAHs. In the experiment of Ekern, no C_2H_2 loss is recorded for fluoranthene, in agreement with the latest work of Jochims et al. [41]. It is not clear whether the acetylene loss requires more or the same energy than the H atom loss. In their study of the naphthalene cation [51] and in another study of size effects on the dissociation of PAHs [26], Jochims et al. have found that the energy necessary for acetylene loss is comparable to the energy for H atom loss. The peak corresponding to C_2H_2 loss is small in Fig. 9, and although a slight increase can be noticed when the fluoranthene flow rate is higher, this peak remains small compared to the $C_{16}H_{10-n}{}^+$ peak for all our experimental conditions. For this reason, the contribution of $C_{14}H_8{}^+$ to the primary ions is neglected.

In a recent study of C–N bond formation in the reaction of N^+ with benzene, Ascenzi et al. [52] have observed the formation of linear cyano daughter ions, of formula up to $H_2C_5N^+$. They have not observed nitrogen insertion into the carbon ring, as is observed with C^+. In Fig. 4, the peak at mass 216 could correspond to $C_{16}NH_{10}{}^+$, with or without ring opening. Its height is such that the branching ratio for the formation of $C_{16}NH_{10}{}^+$ is compatible with the upper limit of what is observed for benzene, e.g. the cross-section for the formation of nitrogen-bearing compounds is 10–1000 times smaller than the cross-section for the direct charge transfer. The peak at mass 230 could be the Van der Waals cluster $(C_{16}H_{10}{\cdot}N_2)^+$. These ions are formed via a bimolecular or termolecular process, and are primary ions.

The primary ions are formed from elementary reactions of fluoranthene with the precursor ions. On this basis, only a limited number of bonds can be broken and formed during this process. For this reason, we think that our primary cations consist of $C_{16}H_{10}{}^+$, $C_{16}NH_{10}{}^+$ and $(C_{16}H_{10}{\cdot}N_2)^+$, which can be more

or less dehydrogenated (a loss of four H atoms is a maximum). Isomerization of fluoranthene into pyrene seems to be excluded, due to the drastic required rearrangement of the molecule.

4.2. The other ions

The other ions that are observed in Fig. 4 can be divided into two groups. On one hand are the fragments of mass less than 202, and on the other hand, the adduct ions, formed from the association of the fragments with neutral fluoranthene.

The hydrocarbon primary ions are formed with an internal energy up to 7.68 eV. This energy is quickly redistributed in the vibration modes by internal conversion and subsequent fragmentation follows. The propensity of fluoranthene to break apart cannot be explained by its $4n = 16$ π-electrons, associated to "anti-aromaticity," as it is nearly as stable as the true PAH it resembles [53]. The reason could be its non-alternating character, that means that two bonds of the pentagonal cycle are single bond like and, therefore, weaker than the other C–C bonds of the molecule. Wang et al. [54] propose that the cleavage of such bonds may occur via a concerted retro-Diels–Alder mechanism or a homolytic cleavage. This would lead to fragments of mass 76 and 126. A concerted retro-Diels–Alder can also be invoked for C_4H_2 loss, giving fragments at mass 50 and 152, and for C_2H_2 loss with ring opening. Other fragments that can be formed by breaking two C–C bonds correspond to mass 163 (C_3H_3 loss) and 189 (CH loss). This latter fragment rapidly reacts with fluoranthene, and is one of the major adduct ion (Fig. 4). As nothing is known about the thermochemistry of $C_{16}NH_{10}^+$ and its possible cyano daughter fragments, it is not clear if the peaks correspond to pure hydrocarbon cations, or if they contain cyano daughter ions too. Rapid hydrogen shifts could also explain, why the peaks on the mass spectrum do not exactly match the expected masses. All other fragment masses require at least three bonds to be broken and the dissociation mechanism remains to be understood.

As soon as the fluoranthene flow rate is not small, the dimer ions represent a large percentage of the cations. Nothing was noticeable in the mass spectrum at masses larger than 500, indicating that only dimers were formed.

4.3. The recombination rates

4.3.1. Primary ions

In our former studies of the recombination of hydrocarbon cations with electrons [36–38,55], all measured recombination rates ranged from 3×10^{-7} to $10 \times 10^{-7} \mathrm{cm^3\,s^{-1}}$, although it was expected to increase with the size of the cation [56].

The fitted value for our primary ions is $25 \times 10^{-7}\,\mathrm{cm^3\,s^{-1}}$ and represents the mean recombination rate for $C_{16}H_{10}^+$, $C_{16}NH_{10}^+$, and $(C_{16}H_{10}{\cdot}N_2)^+$, which can be more or less dehydrogenated. Although $C_{14}H_8^+$ is a primary cation, it is produced in such a little amount that its contribution to the mean recombination rate is negligible. The difference in the recombination rate cannot be explained by the size of the cations formed from fluoranthene, which are not fundamentally different from the largest species studied up to now, which was $C_{15}H_9^+$ [55]. Nitrogen addition to the cation is a minor channel for the reaction N^+ + benzene [52]. The peak observed in our spectrum which is analogous to this channel is smaller than the peak of $C_{16}H_{10}^+$, but the branching ratio could be more than that observed for benzene, or even for naphthalene where such addition is not observed at all [29]. This could be another consequence of the relative fragility of the pentagonal cycle, which could be transformed into a hexagonal heterocycle by N^+ insertion.

Are such ions responsible for the increase of the recombination rate? The dissociative recombination rates of methylammonium $CH_3NH_3^+$ and protonated propanenitrile $C_2H_5CNH^+$ have been found to be $1.4 \times 10^{-6}\,\mathrm{cm^3\,s^{-1}}$ [57] and $4.7 \times 10^{-7}\,\mathrm{cm^3\,s^{-1}}$, respectively [58]. If the latter is close to the recombination rates for hydrocarbon cations of the same size, methylammonium has a recombination rate of the same order of magnitude as our primary ions. These

ions, however, do not represent the largest percentage of our primary ions, and even if their recombination rate is greater than $2.5 \times 10^{-6}\,cm^3\,s^{-1}$, but smaller than the physical limit of $5.3 \times 10^{-6}\,cm^3\,s^{-1}$, it seems reasonable to assume that the pure hydrocarbon primary ions recombine rapidly also, at a rate maybe lower, but close to the mean measured value.

4.3.2. The secondary ions

As indicated before, daughter fragments of the primary ions and adducts ions form the second group of ions, the secondary ions. For the reasons given in Section 3.3, the mean value for their recombination rate is close to the physical limit, that is $1.1 \times 10^{-5}\,cm^3\,s^{-1}$.

The upper value for recombination rates of the fragments can be evaluated to be less than $2 \times 10^{-6}\,cm^3\,s^{-1}$ on the basis of the studies of smaller unsaturated cations. This combined with the fact that their abundance is smaller than the abundance of dimer ions, means that fragments do not contribute very much to the mean experimental value of the dissociative recombination. Dimer cations have, therefore, a very large dissociative recombination rate. Similar behaviours have been found for clusters such as $O_2{\cdot}O_2^+$ ($\alpha = 4.2 \times 10^{-6}\,cm^3\,s^{-1}$ [59]) or $CO_2{\cdot}Na^+$ ($\alpha = 5.0 \times 10^{-6}\,cm^3\,s^{-1}$ [60]) and the recombination rate can reach values greater than $10^{-5}\,cm^3\,s^{-1}$ for proton bridged clusters such as $(H_2O)_6{\cdot}H_3O^+$ [61].

5. Conclusion

We have formed two families of positive ions by charge-transfer reaction between fluoranthene and N^+ and $N_2{}^+$. Their recombination with electrons has been examined by modelling several sets of electron density measurements, the values of the recombination rates being adjustable parameters. The reaction times for ion–molecule reactions between fluoranthene and N^+ and $N_2{}^+$ were measured, as well as the diffusion time for N^+. We obtained a value of $(2.5 \pm 1.5) \times 10^{-6}\,cm^3\,s^{-1}$ for the recombination reaction rate of our primary ions, which consist of $C_{16}H_{10}{}^+$, $C_{16}NH_{10}{}^+$, and $(C_{16}H_{10}{\cdot}N_2)^+$ with different levels of dehydrogenation. As the physical limit for the recombination rate of any of these ions is $5.3 \times 10^{-6}\,cm^3\,s^{-1}$, and as $C_{16}H_{10-n}{}^+$ ions are formed in a greater amount than the nitrogen-bearing ions, one can deduce from this result that $C_{16}H_{10-n}{}^+$ ions recombine faster than any hydrocarbon cation studied up to now. This is the most important result that we can learn from this experiment. The recombination of the dimer cations is even faster and close to the physical limit, but no definitive value can be attributed to this recombination rate at our level of modelling.

Fluoranthene is the first neutral parent for which nitrogen addition by ion–molecule reaction is observed in such proportions. This could be done by inserting the nitrogen atom into the pentagonal ring, thus forming an heterocycle. Comparisons of the dissociative recombination rates of radical cations of nitrogen-bearing heterocycles, such as pyridine, with radical cations of aromatic hydrocarbons, such as benzene, would help to determine in what amount such ions are responsible for the increase of the mean recombination rate.

References

[1] U. Ghosh, J.W. Talley, R.G. Luthy, Environ. Sci. Technol. 35 (17) (2001) 3468.
[2] S. Mollerup, S. Ovrebo, A. Haugen, Int. J. Cancer 92 (1) (2001) 18.
[3] F. Cignoli, S. De Iuliis, G. Zizak, Fuel 80 (2001) 945.
[4] H. Naraoka, A. Shimoyama, K. Harada, Earth Planet Sci. Lett. 184 (2000) 1.
[5] A. Léger, J.L. Puget, Astron. Astrophys. 137 (1984) L5.
[6] A. Léger, L. d'Hendecourt, Astron. Astrophys. 146 (1985) 81.
[7] H.M. Calcote, Combust. Flame 42 (1981) 215.
[8] C.W. Bauschlicher, A. Ricca, Chem. Phys. Lett. 326 (2000) 283.
[9] H.M. Calcote, R.J. Gill, in: H. Bockhorn (Ed.), Soot Formation in Combustion, Springer, Berlin, 1994, p. 471.
[10] M. Frenklach, H. Wang, NTIS report AFOSR-TR-91-0169, 2001, p. 1
[11] D.M. Hudgins, C.W. Bauschlicher, L.J. Allamandola, Spectrochim. Acta A 57 (2001) 907.
[12] G.C. Sloan, T.L. Hayward, L.J. Allamandola, J.D. Bregman, B. Devito, D.M. Hudgins, Astrophys. J. 513 (1999) L65.
[13] T.P. Snow, Spectrochim. Acta A 57 (2001) 615.
[14] L.J. Allamandola, D.M. Hudgins, S.A. Sandford, Astrophys. J. 511 (2) (1999) L115.

[15] C. Moutou, L. Verstraete, K. Sellgren, W. Schmidt, Astron. Astrophys. 354 (2000) L17.
[16] C. Van Kerckhoven, S. Hony, E. Peeters, A.G.G.M. Tielens, L.J. Allamandola, D.M. Hudgins, P. Cox, P.R. Roelfsema, R.H.M. Voors, C. Waelkens, L.B.F.M. Waters, P.R. Wesselius, Astron. Astrophys. 357 (2000) 1013.
[17] C. Joblin, A.G.G.M. Tielens, T.R. Geballe, D.H. Wooden, Astrophys. J. Lett. 460 (1996) L119.
[18] L.J. Allamandola, A.G.G.M. Tielens, J.R. Barker, Astrophys. J. Lett. 290 (1985) L25.
[19] A. Li, B.T. Draine, Astrophys. J. 550 (2) (2001) L213.
[20] M. Benedettini, S. Pezzuto, T. Giannini, D. Lorenzetti, B. Nisini, Astron. Astrophys. 379 (2001) 557.
[21] T. Pino, P. Brechignac, E. Dartois, K. Demyk, L. d'Hendecourt, Chem. Phys. Lett. 339 (1/2) (2001) 64.
[22] N. Boudin, T. Pino, P. Brechignac, J. Mol. Struct. 563/564 (2001) 209.
[23] D. Romanini, L. Biennier, A. Salama, A. Kachanov, L.J. Allamandola, F. Stoeckel, Chem. Phys. Lett. 303 (1999) 165.
[24] J. Oomens, G. Meijer, G. von Helden, J. Phys. Chem. 105 (2001) 8302.
[25] V. Le Page, T.P. Snow, V.M. Bierbaum, Astrophys. J. Suppl. Ser. 132 (2001) 233.
[26] H.W. Jochims, E. Rühl, H. Baumgärtel, S. Tobita, S. Leach, Astrophys. J. 420 (1994) 307.
[27] E. Herbst, V. Le Page, Astron. Astrophys. 344 (1999) 310.
[28] B.R. Rowe, J.C. Gomet, A. Canosa, C. Rebrion-Rowe, J.B.A. Mitchell, J. Chem. Phys. 96 (1992) 1105.
[29] A.J. Midey, S. Williams, S.T. Arnold, I. Dotan, R.A. Morris, A.A. Viggiano, Int. J. Mass Spectrom. Ion Process. 195/196 (2000) 327.
[30] Y. Ikezoe, S. Matsuoka, M. Takabe, A.A. Viggiano, Gas Phase Ion–Molecule Reaction Rates Through 1986, Maruzen Co., Japan, 1987.
[31] W. Lindinger, A.L. Schmeltekopf, F.C. Fehsenfeld, J. Chem. Phys. 61 (7) (1974) 2890.
[32] A. Canosa, J.C. Gomet, B.R. Rowe, J.L. Queffelec, J. Chem. Phys. 94 (1991) 7159.
[33] NIST Standard Reference Database Number 69, The National Institute of Standards and Technology (NIST), http://webbook.nist.gov/, 2001.
[34] S. Laubé, T. Mostefaoui, B.R. Rowe, Rev. Sci. Instrum. 71 (1) (2000) 519.
[35] P. Spanel, L. Dittrichova, D. Smith, Int. J. Mass Spectrom. Ion Phys. 129 (1993) 183.
[36] L. Lehfaoui, C. Rebrion-Rowe, S. Laubé, J.B.A. Mitchell, B.R. Rowe, J. Chem. Phys. 106 (3) (1997) 5406.
[37] C. Rebrion-Rowe, L. Lehfaoui, B.R. Rowe, J.B.A. Mitchell, J. Chem. Phys. 108 (17) (1998) 7185.
[38] C. Rebrion-Rowe, T. Mostefaoui, S. Laubé, J.B.A. Mitchell, J. Chem. Phys. 113 (8) (2000) 3039.
[39] S. Tobita, M. Meincke, E. Illenberger, L.G. Christophorou, H. Baumgärtel, S. Leach, J. Chem. Phys. 161 (1992) 501.
[40] Y. Ling, C. Lifshitz, J. Phys. Chem. 99 (1995) 11074.
[41] H.W. Jochims, E. Rühl, H. Baumgärtel, S. Tobita, S. Leach, Int. J. Mass Spectrom. Ion Process. 167/168 (1997) 35.
[42] D. Smith, N.G. Adams, in: F. Brouillard, J.W. McGowan (Eds.), Physics of Ion–Ion and Electron–Ion Collisions, Plenum Press, New York, 1983, p. 501.
[43] G.D. Chen, R.G. Cooks, J. Mass Spectrom. 30 (8) (1995) 1167.
[44] L.G. Christophorou, R.P. Blaunstein, Radic. Res. 37 (1969) 229.
[45] T. Mostefaoui, C. Rebrion-Rowe, J.L. Le Garrec, B.R. Rowe, J.B.A. Mitchell, Faraday Discuss. 109 (1998) 71.
[46] A. Omont, Astron. Astrophys. 164 (1986) 159.
[47] L. Verstraete, A. Léger, L. d'Hendecourt, O. Dutuit, D. Défourneau, Astron. Astrophys. 237 (1990) 436.
[48] L. Spitzer, Physical Processes in the Interstellar Medium, Wiley, New York, 1978.
[49] M. Rubio, J. Sánchez-Marín, E. Ortí, Synth. Metals 71 (1995) 2081.
[50] S.P. Ekern, A.G. Marshall, J. Szczepanski, M. Vala, J. Phys. Chem. A 102 (1998) 3498.
[51] H.W. Jochims, H. Rasekh, E. Rühl, H. Baumgärtel, S. Leach, Chem. Phys. 168 (1992) 159.
[52] D. Ascenzi, P. Franceschi, T.G.M. Freegarde, P. Tosi, D. Bassi, Chem. Phys. Lett. 346 (2001) 35.
[53] S.W. Slayden, J.F. Liebman, Chem. Rev. 101 (2001) 1541.
[54] X. Wang, H. Becker, A.C. Hopkinson, R.E. March, L.T. Scott, D.K. Böhme, Int. J. Mass Spectrom. Ion Phys. 161 (1997) 69.
[55] B.R. Rowe, C. Rebrion-Rowe, in: D. Zajfman, J.B.A. Mitchell, D. Schwalm, B.R. Rowe (Eds.), Dissociative Recombination: Theory, Experiment and Applications III, World Scientific Publishing, 1996.
[56] J.B.A. Mitchell, J. Miller, Combust. Flame 75 (1989) 45.
[57] N.G. Adams, D. Smith, Chem. Phys. Lett. 144 (1988) 11.
[58] M. Geoghegan, N.G. Adams, D. Smith, J. Phys. B 24 (1992) 2589.
[59] J.L. Dulaney, M.A. Biondi, R. Johnsen, Phys. Rev. A 24 (1988) 743.
[60] G.E. Keller, R.A. Beyer, J. Geophys. Res. 76 (1971) 289.
[61] M.T. Leu, M.A. Biondi, R. Johnsen, Phys. Rev. A 7 (1973) 292.